Chapter 12

Directly Probing the Phase States and Surface Tension of Individual Submicrometer Particles Using Atomic Force Microscopy

Hansol D. Lee, Kamal K. Ray, and Alexei V. Tivanski*

Department of Chemistry, University of Iowa, Iowa City, Iowa 52242, United States
***E-mail: alexei-tivanski@uiowa.edu**

Large uncertainties still remain in our ability to accurately predict the overall aerosol effect on the climate and atmosphere. One reason for this comes from the paucity of relevant experimental data for submicrometer-sized aerosol particles that can be in solid, semisolid, and liquid phases. Therefore, this becomes a multiphase chemistry problem that requires experimental techniques to overcome the inherent size limitations currently present in the scientific community and directly measure atmospherically relevant physical-chemical properties of aerosols. Here, we review the latest atomic force microscopy (AFM) based methodologies that provide the capability to identify the 3D morphology of aerosol particles and directly probe their important properties on a single particle basis. Herein the focus is on two physical-chemical properties of model aerosol systems: phase state and surface tension. Novel nanoindentation and nano-Wilhelmy AFM techniques are used to directly measure the two properties, while modulating the relative humidity and thus controlling the concentration and viscosity. Overall, the established methodologies discussed herein can be used to better understand the role of multiphase aerosols on the climate and atmosphere.

Hunt et al.; Multiphase Environmental Chemistry in the Atmosphere
ACS Symposium Series; American Chemical Society: Washington, DC, 2018.

Introduction

Our world is full of aerosols that are more than a thousand times smaller than a single human hair strand. These small and perhaps even seemingly harmless aerosols, or particles, can have a paradoxically large impact on the climate. In the atmosphere, they can contribute to global cooling directly by reflecting the solar radiation and indirectly by seeding clouds (*1–4*). Examples of these primary particles can include mineral dust, volcanic ash, soot, and sea spray aerosols. Secondary aerosol particles also exist and form from volatile compounds that underwent chemical reactions that define their size, shape, and composition. A well-known example is secondary organic aerosols (*5–13*).

These aerosols of diverse origins in nature are chemically and physically complex. At first, the former may seem more intuitive than the latter; aerosols that come from trees have different chemical makeup in comparison to those that come from the ocean or a volcano. But what about physical complexity? The scientific community now understands that, sometimes due to the significant amount of oxygenated organic compounds in aerosols, the phase state (solid, semisolid, and liquid) can vary from particle-to-particle, depend on source, and vary as a function of relative humidity (RH) and temperature (*7*, *14–17*). This variability is in direct opposition to our simplified assumption, which we held in the past decades, that organic aerosols regardless of origin or atmospheric conditions were liquid in phase state (*18*).

The implication of this relatively new discovery is the following: from both experimental and theoretical perspective, the varying particle phase states bring a new dimension to an already difficult problem of accurately predicting the overall aerosol effect on the climate and atmosphere. Thus, our ability to accurately represent this complexity both experimentally and theoretically is absolutely paramount, and it must be done in a manner in which the small, yet unique, differences of individual particles are fully represented, instead of being simplified by being averaged out in an ensemble of a countless number of particles. An example of when this individual particle information is needed is atmospherically relevant particles, where only one out of a million particles actually form ice clouds and globally cool the climate (*19*, *20*). We therefore need to explore single particle techniques that can measure atmospherically relevant, physical-chemical properties of aerosols.

To better understand the implications that arise from the physical-chemical heterogeneity of individual aerosols, we now see a relatively new avenue of scientific research that specifically focuses on studying one particle at a time. For example, single particle experimental techniques such as atomic force microscopy (AFM) can uniquely study submicrometer-sized (less than 1 micrometer in size) particles, by imaging their 3D morphology and measuring the interaction forces with picoNewton force sensitivity that can be related to their physical-chemical properties. AFM uses a sharp probe or a tip, typically 2 – 10 nm at the apex, in order to raster scan over the surface (*21–25*). In 2016, AFM was used, for the very first time, to directly quantify the hygroscopic growth, or increase in the size of a substrate-deposited particle due to water uptake, on an individual particle basis at room temperature and varying RH (Figure 1A) (*26*). When comparing the

individual particle AFM water uptake data to bulk ensemble average data from a conventional hygroscopic tandem differential mobility analyzer (HTDMA), where the width of the Gaussian average reflects particle-to-particle variability, the AFM showed higher sensitivity to particle-to-particle diversity that revealed a correlation between 3D morphology and hygroscopic growth (Figure 1B, D). The bulk ensemble data from the HTDMA on the other hand, returned one "representative" average value (Figure 1C). Overall, the water uptake response from substrate-deposited particles measured with the AFM is in agreement with the HTDMA results collected for airborne particles. In other words, the presence of the substrate for the AFM measurements did not alter the water uptake property of the aerosol particle. Following the successful demonstration of the AFM ability to quantitatively measure water uptake of individual particles as a function of RH prompted us to further develop the technique to study important physical-chemical properties of aerosols: physical phase state and surface tension. Both have strong significance to how aerosols affect the climate and also evolve due to the variation of atmospheric RH that modulates the water uptake and subsequently changes the concentration and viscosity.

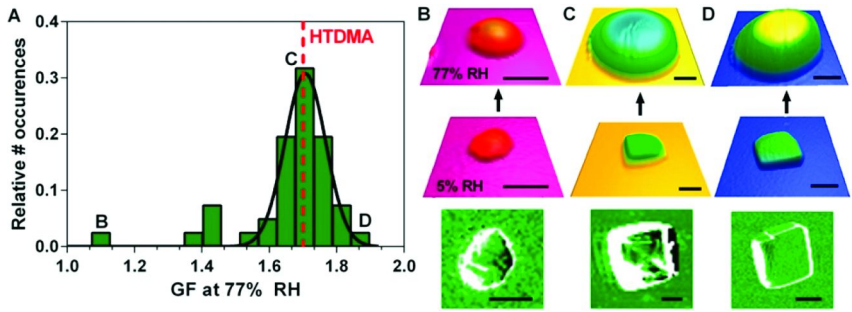

Figure 1. (A) Volume growth factor (GF) at 77% RH distribution measured for 40 individual nonanoic acid/NaCl particles. The data was fit to a Gaussian distribution. The red dashed line labels the GF value determined with HTDMA. Letters correspond to particles shown in (B)–(D). (B–D) The middle row of images shows dehydrated particles at 5% RH and corresponding deliquesced liquid droplets at 77% RH are shown above. The bottom row is phase images. (B) corresponds to the extreme left side of the distribution of GFs, while (C) corresponds to the most probable GF value and is representative of the majority of particles. (D) corresponds to the extreme right side of the GFs distribution. All scale bars are 500 nm. Reprinted with permission from (Reference (26)). Copyright (2016) American Chemical Society.

In this chapter, we review the latest works that have further developed the AFM techniques to directly measure atmospherically relevant properties, such as phase state and surface tension of individual particles. Here, sucrose is used as an ideal model system because of its access to all phase states at subsaturated RH (below 100%) and its quantified relationship between RH, solute concentration,

and viscosity (*27*, *28*). Following a brief introduction of each property of interest, we show two methodologies that, with minimal modeling and assumptions, are then used to interpret the force profile data collected from AFM. The two methodologies are called nanoindentation and nano-Wilhelmy methods, which use the AFM probe to directly interact with the sucrose particle, and record the particle response to the applied mechanical force. The response is then used to both qualitatively and quantitatively determine the phase state and surface tension at varying RH. We conclude by suggesting future research directions from this established work that involve applying these methodologies to highly complex nascent aerosol systems, to further improve our understanding of how aerosols influence our world by using novel microscopy techniques such as the AFM.

Discussion

Assessment of the Particle Phase States with Hygroscopic Growth

Particle phase state can dictate water uptake, determine whether particles can help form clouds, and control the chemical reactivity with gas phase molecules in the atmosphere (*17*, *29–34*). This is especially important to understand for submicrometer-sized particles that can last a much longer time (up to weeks) in the atmosphere than supermicrometer sized aerosols (*35*). However, the small particle size has been limiting experimental capabilities to directly measure the phase state until very recently. Here, we review the latest AFM technique that directly identifies the phase state of submicrometer-sized particles, with minimal modeling and assumptions used (*36*). The AFM nanoindentation technique uses a sharp (typically several to tens of nanometers) tip that presses into a substrate deposited particle with a specific amount of applied force and records the resulting particle response to establish mechanical equilibrium as a function of RH. The quantitative analysis is used to interpret the force profile or force spectroscopy, which is a collection of force *versus* tip-sample separation data, to quantify the viscoelastic response distance (VRD) and relative indentation depth (RID). These two measurements are newly established means of assessing the phase state of individual sucrose particles which may vary with RH, from solid, semisolid, and liquid phase, or the corresponding viscosity range from 10^{16} to 10^{-3} Pa s, respectively.

To modulate the viscosity of sucrose, a humidity cell is used to control the RH, and thus the concentration of the particles. In hydration mode, the particle grows in size and height from the increased RH, and this growth can be directly observed using 3D AFM imaging. In Figure 2A, the AFM 3D height image of a single sucrose particle at varying RH is shown, where the left and right images are at 4% and 80% RH, respectively. Thus, by increasing the RH from 4% to 80%, the particle grows from ~500 nm to ~700 nm in diameter. To quantify the water uptake behavior, volume-equivalent growth factor (GF) is calculated by the ratio of the wet volume-equivalent diameter divided by the dry volume-equivalent diameter, recorded at ~4% RH, which is shown in Figure 2B. Single particle data show that the sucrose particle has a continuous water uptake at subsaturated RH

range, which agrees well with the theoretical prediction from the aerosol inorganic-organic mixtures functional groups activity coefficients (AIOMFAC) models (*37*). The hydration step is performed to modulate the viscosity and concentration, and then to identify the phase states on a single particle basis by observing the particle response to applied force (Figure 3). The same idea is also used for the AFM-based surface tension measurements, as discussed in a later section.

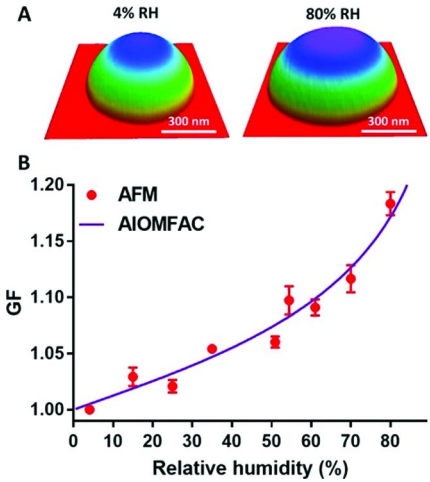

Figure 2. (A) AFM 3D height images of sucrose particle at 4% and 80% RH. As the RH is increased, the particle uptakes water and grows in size, from ~500 nm in diameter and 250 nm in height at 4% RH to ~700 nm in diameter and 300 nm in height at 80% RH. (B) AFM hydration volume-equivalent growth factor versus RH. Red circles with error bars represent average AFM growth factor data and two standard deviations. Purple line represents theoretical prediction of the GF using the AIOMFAC model (15). Reprinted with permission from (Reference (36)). Copyright (2017) American Chemical Society.

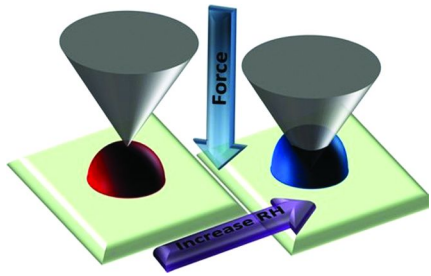

Figure 3. Representation of AFM probe applying predefined force onto a particle at varying RH. Reprinted with permission from (Reference (36)). Copyright (2017) American Chemical Society.

RH identification for the phase transition between solid and semisolid phase is not expected to be as discrete as that for the solid-to-liquid transition; instead, a smooth and relatively small change is expected. However, force spectroscopy measurements over an individual particle after 3D imaging can quantify both the phase state and surface tension. Figure 4 shows several representative examples of forces acting onto the AFM probe as a function of tip–sample separation (TSS), which is the experimentally obtainable distance between the tip and the top surface of the sucrose particle. With decreasing TSS, the probe comes down from the z-direction perpendicular to the particle surface, until there is a mechanical contact with the particle, with continued downward motion into and through the particle resulting in an indentation until a predefined maximum force is reached. After reaching the predefined maximum force, the AFM probe reverses in direction and retracts away from the particle and towards its original starting position above the particle. Within the force profiles data, the phase transition between solid and semisolid phase state was determined by observing the viscoelastic response distance, or the hysteresis distance between the approach and retract force curves in the contact region, from 7% to 19% RH (Figure 4A). Increasing hysteresis indicates that the sucrose particle has undergone transition from purely elastic to viscoelastic material, which shows both viscous and elastic behaviors when being deformed. This is normalized at the 0 nN force position on the force profile. Data show that for the sucrose particle at 7% RH, the VRD is 0.2 ± 0.1 nm, and shows a small increase to 0.4 ± 0.3 nm at 15% RH. At 19% RH, the VRD is 0.6 ± 0.2 nm, which is now statistically different relative to the expected uncertainty in the VRD value (~ 0.2 nm). Thus, the phase transition between solid and semisolid can be determined to be at ~18% RH, which corresponds to the viscosity value of $10^{11.2}$ Pa s. This agrees well with the currently accepted value of 10^{12} Pa s from multiple sources in the literature (*38*, *39*).

The transition from semisolid to liquid can also be determined from the force profiles data, by observing the change in the indentation depth with varying RH. At 54% RH, the approach force curve does not show significant indentation from the observed negative shallow slope with continued decrease in the TSS with increase in force (Figure 4B). Upon increasing the RH to 61%, however, the approach curve shows a drastically different response with the AFM tip indenting completely through the particle at the given maximum applied force, and touching the substrate underneath the particle. This is evident from the approach curve with the slope becoming almost perpendicular after the initial contact, thus indicating a phase transition from semisolid to liquid. Therefore, this type of the data can be used as a qualitative means to predict the semisolid to liquid transition, which should be at around 60% RH, or viscosity of $10^{2.5}$ Pa s for sucrose (*39*).

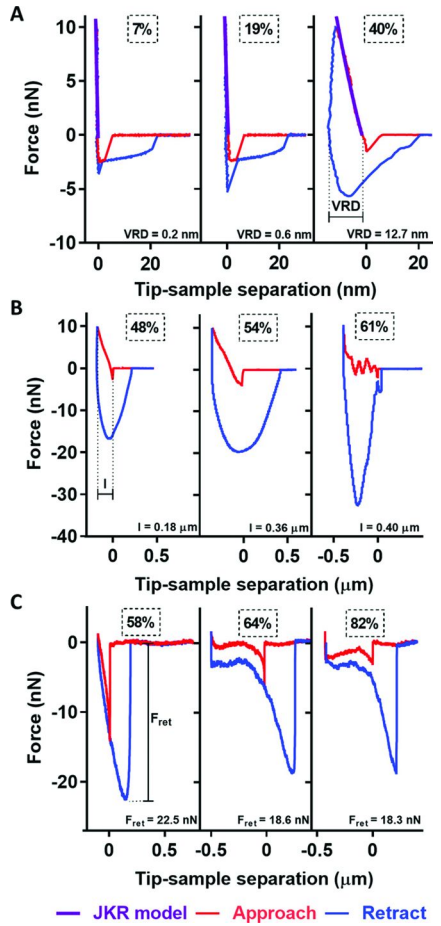

Figure 4. Force versus tip–sample separation plots for selected RH ranging from 7% to 82% of a sucrose particle. Tip sample separation of 0 indicates the initial position of AFM tip contact with the surface of the particle. The evolution of the force profiles from low to high RH is shown from left to right, using x-offset. Red lines indicate approach to the sucrose particle, and blue lines retract away from the particle. The purple lines indicate the JKR model fit in the contact region. (A) Force profiles at 7%, 19%, and 40% RH collected at the maximum applied force of 10 nN. The corresponding viscoelastic response distance (VRD) is specified below. (B) Force profiles at 48%, 54%, and 61% RH collected at the maximum applied force of 10 nN. The corresponding indentation depth (I) is specified below. (C) Force profiles at 58%, 64%, and 82% RH collected at the maximum applied force of 1 nN. The retention force (F_{ret}) used to calculate surface tension is specified below. Reprinted with permission from (Reference (36)). Copyright (2017) American Chemical Society.

To further accurately assess the semisolid to liquid phase transition of sucrose, the quantitative measure of relative indentation depth at varying RH is developed and employed. This unitless value at a particular RH is defined as the following:

$$RID = \frac{I}{H} \tag{1}$$

where I is the indentation depth that represents total distance that the AFM probe moves in the z-direction from the top surface of the particle to the depth indented into the particle and H is the maximum height of the particle. A low relative indentation depth value would thus represent a dehydrated and mechanically stiff particle that resists the AFM tip to indent significantly into the particle, and vice versa (Figure 4B, C). The result is shown in Figure 5A, where the combination of both viscoelastic response distance and relative indentation depth at varying RH and viscosity are shown. Due to high viscosity from 7% to 34% RH range, the measured RID is small at ~0.04. RID does not significantly increase until 44% RH, where beyond this RH value, the sucrose viscosity becomes low enough that the AFM probe makes an appreciable amount of indentation into the particle in comparison to its maximum height. Further increase to 47% RH, RID is approximately 0.18, and leading up to the previously proposed transition point at 60% RH, the RID becomes 0.98 and the particle now behaves like a liquid droplet. This transition, in comparison to the solid and semisolid phase state, is not discrete but continuous. Increase in RH beyond 60% shows RID plateauing to the value of 1, where the indentation depth and particle height becomes equal to each other. Further study was designed to determine whether experimental parameters such as applied force affects the relative indentation depth measurements, which indicated that the phase state measurements from the AFM are unaffected by varying applied force, as long as the maximum force value of 5 nN and higher is used (Figure 5B).

Surface Tension Assessment of Liquid Phase Droplets

To theoretically predict cloud formation by atmospheric aerosols, κ-Köhler theory and compressed film theory are often used (*40*, *41*). A key factor in both, however, is the surface tension of the aerosol droplet, where the present assumption is a fixed value equal to that of pure water (72.8 mN/m at 25 ºC). However, aerosols often contain surface-active compounds that can significantly decrease the surface tension of the aerosol droplet, thus challenging the validity of the constant surface tension assumption (*42*, *43*). These models are expected to be significantly improved in their accuracy if direct surface tension measurements of relevant aerosol particles are provided to establish accurate and relevant surface tension value ranges for nascent particles with diverse chemical compositions and origin.

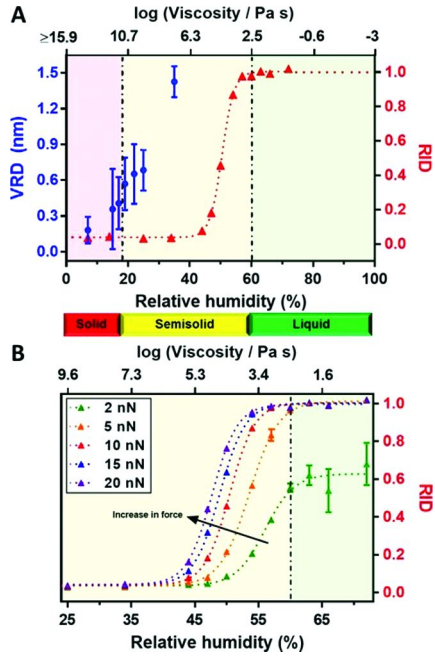

Figure 5. (A) AFM viscoelastic response distance (VRD, left, blue circles) and relative indentation depth (RID, right, red triangles) versus RH and corresponding viscosity collected with 10 nN of maximum applied force. The error bars represent two standard deviations for the VRD and RID, although sometimes smaller than the symbol. The RH–viscosity relationship is taken from Song et al. The red dotted line is shown for clarity and represents the fit using a four-parameter logistic sigmoidal function. Color bars indicate the various phase states of the sucrose particle at given RH from solid, semisolid, and liquid. The dashed black lines represent phase transition points determined by the force profiles of sucrose. The phase transition from solid to semisolid states occurred at ~18% RH and $10^{11.2}$ Pa s, while the semisolid to liquid state transition occurred at ~60% RH and $10^{2.5}$ Pa s. (B) RID versus RH and corresponding viscosity from 25% to 70% RH with varying maximum applied forces from 2 to 20 nN. The colored dotted lines are shown for clarity and represent the fit using a four-parameter logistic sigmoidal function. Reprinted with permission from (Reference (36)). Copyright (2017) American Chemical Society.

Here, we review the latest AFM technique that directly measures the surface tension of submicrometer-sized particles (*43*, *44*). With a constant radius AFM nanoneedle, nano-Wilhelmy method is used to probe the substrate-deposited particle with the nanoneedle, which measures the retention force required to break the formed meniscus between the droplet and the nanoneedle as a function of RH (Figure 6). The approach is nearly identical to the Wilhelmy plate method, which uses a macro-sized needle to immerse into the liquid, and measure the force required to break the meniscus. This force is used to quantify the surface tension.

The general expression for surface tension is defined as force over unit length for a bulk solution. Extending this to the nano-Wilhelmy method applicable for this methodology, the equation for surface tension is expressed as the following:

$$\sigma = \frac{F_{ret}}{2\pi r} \tag{2}$$

where F_{ret} is the retention force and r is radius of the nanoneedle. Similar to phase state measurements, this methodology is repeated after 3D particle imaging as a function of increasing RH. As RH increases, the particle uptakes more water and becomes more dilute, decreasing the solute concentration which then changes the surface tension. The force spectroscopy is used to measure the retention force (Figure 4C) for the RH range where sucrose particle is liquid in phase.

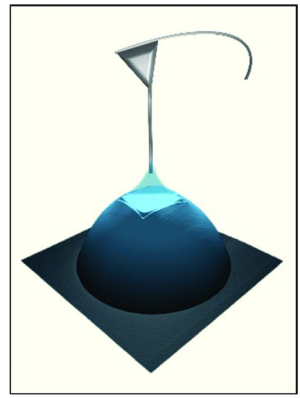

Figure 6. Representation of AFM nanoneedle probe applying predefined force onto a particle and measuring the retention force from the meniscus. Reprinted with permission from (Reference (43)). Copyright (2017) American Chemical Society.

As an example, AFM 3D height image of a glucose particle at ~20% RH is shown (Figure 7A); sucrose also displays similar rounded morphology. The surface tension result for sucrose is shown in Figure 7B, where single particle surface tension measurements are shown in blue circles with error bars, indicating two standard deviations. The red dashed line indicates surface tension prediction from bulk solution surface tension measurements. The bulk surface tension data collected with the conventional Wilhelmy plate method, used to measure the surface tension value of liquids approximately 4 mL in volume. Within the experimentally identified RH range, there is a good overlap between the AFM and bulk surface tension data, despite the individual particles being submicrometer in size. The good overlap is also seen even below ~70% RH, the solubility point of sucrose, when the particle is becoming supersaturated in concentration. However, if the RH is to go even lower, enough to undergo a phase transition from liquid to semisolid below 60% RH, the measured retention force now has a strong

viscosity contribution that cannot be decoupled, and the resultant surface tension will deviate in comparison to the bulk trend line.

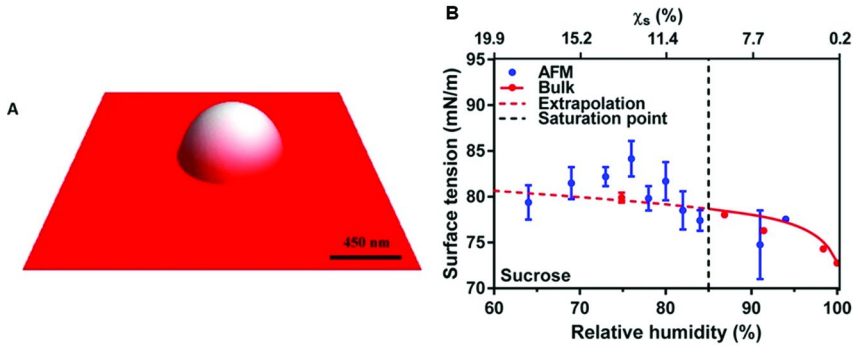

Figure 7. Representative AFM 3D height image at ~20% RH of glucose particle with height of ~350 nm (A). Surface tension vs RH (bottom axis) and corresponding solute mole percentage (top horizontal axis) for ~600 nm diameter sucrose (blue circles with error bars) (B). Average AFM surface tension data and two standard deviations. (red circles) Bulk solution surface tension measurements. Because of the low standard deviation, the error bars for the bulk data are smaller than the size of the symbol. Red solid line is the bulk trend line. Red dashed line is the extrapolation of the bulk trend line above the saturation point, which is indicated by the vertical black dashed line. Reprinted with permission from (Reference (43)). Copyright (2017) American Chemical Society.

Conclusions

In this review, we assessed new AFM methodologies that directly measure as a function of relative humidity, atmospherically relevant physical-chemical properties including the phase state and surface tension, of individual submicrometer-sized substrate-deposited particles. Complementary AFM nanoindentation and nano-Wilhelmy methodologies were used to collect forces acting on the AFM tip *versus* tip-sample separation profiles at varying RH that were then interpreted to quantify the two properties at subsaturated RH. For qualitative and quantitative assessment of the phase states, AFM methods revealed distinct changes in the phase state within viscosity ranges from 10^{16} to 10^{-3} Pa s for sucrose. Three different phase states of an individual sucrose particle corresponding to solid, semisolid, and liquid states were accessed and quantified. In the future, this approach can be further developed to determine the particle phase states of other atmospherically relevant chemical systems, at varying mixing states and increased complexity. In this regard, nascent aerosol particles collected on a substrate may be characterized for their phase states at a specific RH. AFM was used to also directly measure the surface tension of individual submicrometer sucrose particles at ambient temperature and varying RH conditions. The single particle AFM data overlap well with the bulk surface tension values when the particle phase state is liquid. In the future, applying this

methodology to measure the surface tension of more complex particles, such as nascent aerosols of unknown composition, would provide further insights into the extent of particle-to-particle surface tension variation for aerosols of different origins, ultimately improving our understanding of the factors that facilitate cloud formation at a specific RH. With further developmental progress, this may allow us to elucidate the multiphase role of various aerosols on the climate and atmosphere.

Acknowledgments

This work was funded by the National Science Foundation through the Center for Aerosol Impacts on Chemistry of the Environment under grant no. CHE 1305427. Any opinions, findings, and conclusions or recommendations expressed in this material are those of the authors and do not necessarily reflect the views of the National Science Foundation.

References

1. Haywood, J.; Boucher, O. Estimates of the direct and indirect radiative forcing due to tropospheric aerosols: A review. *Rev. Geophys.* **2000**, *38*, 513–543.
2. Fuentes, E.; Coe, H.; Green, D.; de Leeuw, G.; McFiggans, G. Laboratory-generated primary marine aerosol via bubble-bursting and atomization. *Atmos. Meas. Tech.* **2010**, *3*, 141–162.
3. Jacobson, M. Z. Global direct radiative forcing due to multicomponent anthropogenic and natural aerosols. *J. Geophys. Res.-Atmos.* **2001**, *106*, 1551–1568.
4. de Leeuw, G.; Andreas, E. L.; Anguelova, M. D.; Fairall, C. W.; Lewis, E. R.; O'Dowd, C.; Schulz, M.; Schwartz, S. E. Production Flux of Sea Spray Aerosol. *Rev. Geophys.* **2011**, *49*, RG2001.
5. Calvo, A. I.; Alves, C.; Castro, A.; Pont, V.; Vicente, A. M.; Fraile, R. Research on aerosol sources and chemical composition: Past, current and emerging issues. *Atmos. Res.* **2013**, *120-121*, 1–28.
6. Fuzzi, S.; Baltensperger, U.; Carslaw, K.; Decesari, S.; Denier van der Gon, H.; Facchini, M. C.; Fowler, D.; Koren, I.; Langford, B.; Lohmann, U.; Nemitz, E.; Pandis, S.; Riipinen, I.; Rudich, Y.; Schaap, M.; Slowik, J. G.; Spracklen, D. V.; Vignati, E.; Wild, M.; Williams, M.; Gilardoni, S. Particulate matter, air quality and climate: lessons learned and future needs. *Atmos. Chem. Phys.* **2015**, *15*, 8217–8299.
7. Saukko, E.; Lambe, A. T.; Massoli, P.; Koop, T.; Wright, J. P.; Croasdale, D. R.; Pedernera, D. A.; Onasch, T. B.; Laaksonen, A.; Davidovits, P.; Worsnop, D. R.; Virtanen, A. Humidity-dependent phase state of SOA particles from biogenic and anthropogenic precursors. *Atmos. Chem. Phys.* **2012**, *12*, 7517–7529.
8. Song, M. J.; Liu, P. F. F.; Hanna, S. J.; Zaveri, R. A.; Potter, K.; You, Y.; Martin, S. T.; Bertram, A. K. Relative humidity-dependent viscosity of

secondary organic material from toluene photo-oxidation and possible implications for organic particulate matter over megacities. *Atmos. Chem. Phys.* **2016**, *16*, 8817–8830.
9. Koop, T.; Bookhold, J.; Shiraiwa, M.; Poschl, U. Glass transition and phase state of organic compounds: dependency on molecular properties and implications for secondary organic aerosols in the atmosphere. *Phys. Chem. Chem. Phys.* **2011**, *13*, 19238–19255.
10. Virtanen, A.; Joutsensaari, J.; Koop, T.; Kannosto, J.; Yli-Pirila, P.; Leskinen, J.; Makela, J. M.; Holopainen, J. K.; Poschl, U.; Kulmala, M.; Worsnop, D. R.; Laaksonen, A. An amorphous solid state of biogenic secondary organic aerosol particles. *Nature* **2010**, *467*, 824–827.
11. Baustian, K. J.; Wise, M. E.; Jensen, E. J.; Schill, G. P.; Freedman, M. A.; Tolbert, M. A. State transformations and ice nucleation in amorphous (semi-)solid organic aerosol. *Atmos. Chem. Phys.* **2013**, *13*, 5615–5628.
12. Perraud, V.; Bruns, E. A.; Ezell, M. J.; Johnson, S. N.; Yu, Y.; Alexander, M. L.; Zelenyuk, A.; Imre, D.; Chang, W. L.; Dabdub, D.; Pankow, J. F.; Finlayson-Pitts, B. J. Nonequilibrium atmospheric secondary organic aerosol formation and growth. *Proc. Natl. Acad. Sci. U.S.A.* **2012**, *109*, 2836–2841.
13. Schill, G. P.; Tolbert, M. A. Heterogeneous Ice Nucleation on Simulated Sea-Spray Aerosol Using Raman Microscopy. *J. Phys. Chem. C* **2014**, *118*, 29234–29241.
14. Wang, B. B.; O'Brien, R. E.; Kelly, S. T.; Shilling, J. E.; Moffet, R. C.; Gilles, M. K.; Laskin, A. Reactivity of Liquid and Semisolid Secondary Organic Carbon with Chloride and Nitrate in Atmospheric Aerosols. *J. Phys. Chem. A* **2015**, *119*, 4498–4508.
15. Hodas, N.; Zuend, A.; Mui, W.; Flagan, R. C.; Seinfeld, J. H. Influence of particle-phase state on the hygroscopic behavior of mixed organic-inorganic aerosols. *Atmos. Chem. Phys.* **2015**, *15*, 5027–5045.
16. Tong, H. J.; Reid, J. P.; Bones, D. L.; Luo, B. P.; Krieger, U. K. Measurements of the timescales for the mass transfer of water in glassy aerosol at low relative humidity and ambient temperature. *Atmos. Chem. Phys.* **2011**, *11*, 4739–4754.
17. Shiraiwa, M.; Ammann, M.; Koop, T.; Poschl, U. Gas uptake and chemical aging of semisolid organic aerosol particles. *Proc. Natl. Acad. Sci. U.S.A.* **2011**, *108*, 11003–11008.
18. Cappa, C. D.; Lovejoy, E. R.; Ravishankara, A. R. Evidence for liquid-like and nonideal behavior of a mixture of organic aerosol components. *Proc. Natl. Acad. Sci. U.S.A.* **2008**, *105*, 18687–18691.
19. DeMott, P. J.; Hill, T. C. J.; Petters, M. D.; Bertram, A. K.; Tobo, Y.; Mason, R. H.; Suski, K. J.; McCluskey, C. S.; Levin, E. J. T.; Schill, G. P.; Boose, Y.; Rauker, A. M.; Miller, A. J.; Zaragoza, J.; Rocci, K.; Rothfuss, N. E.; Taylor, H. P.; Hader, J. D.; Chou, C.; Huffman, J. A.; Poschl, U.; Prenni, A. J.; Kreidenweis, S. M. Comparative measurements of ambient atmospheric concentrations of ice nucleating particles using multiple immersion freezing methods and a continuous flow diffusion chamber. *Atmos. Chem. Phys.* **2017**, *17*, 11227–11245.

20. DeMott, P. J.; Hill, T. C. J.; McCluskey, C. S.; Prather, K. A.; Collins, D. B.; Sullivan, R. C.; Ruppel, M. J.; Mason, R. H.; Irish, V. E.; Lee, T.; Hwang, C. Y.; Rhee, T. S.; Snider, J. R.; McMeeking, G. R.; Dhaniyala, S.; Lewis, E. R.; Wentzell, J. J. B.; Abbatt, J.; Lee, C.; Sultana, C. M.; Ault, A. P.; Axson, J. L.; Martinez, M. D.; Venero, I.; Santos-Figueroa, G.; Stokes, M. D.; Deane, G. B.; Mayol-Bracero, O. L.; Grassian, V. H.; Bertram, T. H.; Bertram, A. K.; Moffett, B. F.; Franc, G. D. Sea spray aerosol as a unique source of ice nucleating particles. *Proc. Natl. Acad. Sci. U.S.A.* **2016**, *113*, 5797–5803.
21. Woodward, X.; Kostinski, A.; China, S.; Mazzoleni, C.; Cantrell, W. Characterization of Dust Particles' 3D Shape and Roughness with Nanometer Resolution. *Aerosol Sci. Tech.* **2015**, *49*, 229–238.
22. Chou, C.; Formenti, P.; Maille, M.; Ausset, P.; Helas, G.; Harrison, M.; Osborne, S. Size distribution, shape, and composition of mineral dust aerosols collected during the African Monsoon Multidisciplinary Analysis Special Observation Period 0: Dust and Biomass-Burning Experiment field campaign in Niger, January 2006. *J. Geophys. Res.-Atmos.* **2008**, *113*, D00C10.
23. Helas, G.; Andreae, M. O. Surface features on Sahara soil dust particles made visible by atomic force microscope (AFM) phase images. *Atmos. Meas. Tech.* **2008**, *1*, 1–8.
24. Li, W. J.; Shao, L. Y.; Zhang, D. Z.; Ro, C. U.; Hu, M.; Bi, X. H.; Geng, H.; Matsuki, A.; Niu, H. Y.; Chen, J. M. A review of single aerosol particle studies in the atmosphere of East Asia: morphology, mixing state, source, and heterogeneous reactions. *J. Clean. Prod.* **2016**, *112*, 1330–1349.
25. Barkay, Z.; Teller, A.; Ganor, E.; Levin, Z.; Shapira, Y. Atomic force and scanning electron microscopy of atmospheric particles. *Microsc. Res. Tech.* **2005**, *68*, 107–114.
26. Morris, H. S.; Estillore, A. D.; Laskina, O.; Grassian, V. H.; Tivanski, A. V. Quantifying the Hygroscopic Growth of Individual Submicrometer Particles with Atomic Force Microscopy. *Anal. Chem.* **2016**, *88*, 3647–3654.
27. Song, Y. C.; Haddrell, A. E.; Bzdek, B. R.; Reid, J. P.; Barman, T.; Topping, D. O.; Percival, C.; Cai, C. Measurements and Predictions of Binary Component Aerosol Particle Viscosity. *J. Phys. Chem. A* **2016**, *120*, 8123–8137.
28. Bones, D. L.; Reid, J. P.; Lienhard, D. M.; Krieger, U. K. Comparing the mechanism of water condensation and evaporation in glassy aerosol. *Proc. Natl. Acad. Sci. U.S.A.* **2012**, *109*, 11613–11618.
29. Kuwata, M.; Martin, S. T. Phase of atmospheric secondary organic material affects its reactivity. *Proc. Natl. Acad. Sci. U.S.A.* **2012**, *109*, 17354–17359.
30. Renbaum-Wolff, L.; Grayson, J. W.; Bateman, A. P.; Kuwata, M.; Sellier, M.; Murray, B. J.; Shilling, J. E.; Martin, S. T.; Bertram, A. K. Viscosity of alpha-pinene secondary organic material and implications for particle growth and reactivity. *Proc. Natl. Acad. Sci. U.S.A.* **2013**, *110*, 8014–8019.
31. Murray, B. J.; Wilson, T. W.; Dobbie, S.; Cui, Z. Q.; Al-Jumur, S. M. R. K.; Mohler, O.; Schnaiter, M.; Wagner, R.; Benz, S.; Niemand, M.; Saathoff, H.; Ebert, V.; Wagner, S.; Karcher, B. Heterogeneous nucleation of ice particles on glassy aerosols under cirrus conditions. *Nat. Geosci.* **2010**, *3*, 233–237.

32. Mikhailov, E.; Vlasenko, S.; Martin, S. T.; Koop, T.; Poschl, U. Amorphous and crystalline aerosol particles interacting with water vapor: conceptual framework and experimental evidence for restructuring, phase transitions and kinetic limitations. *Atmos. Chem. Phys.* **2009**, *9*, 9491–9522.
33. Shiraiwa, M.; Berkemeier, T.; Schilling-Fahnestock, K. A.; Seinfeld, J. H.; Poschl, U. Molecular corridors and kinetic regimes in the multiphase chemical evolution of secondary organic aerosol. *Atmos. Chem. Phys.* **2014**, *14*, 8323–8341.
34. Berkemeier, T.; Huisman, A. J.; Ammann, M.; Shiraiwa, M.; Koop, T.; Poschl, U. Kinetic regimes and limiting cases of gas uptake and heterogeneous reactions in atmospheric aerosols and clouds: a general classification scheme. *Atmos. Chem. Phys.* **2013**, *13*, 6663–6686.
35. Gong, S. L.; Barrie, L. A.; Blanchet, J. P. Modeling sea-salt aerosols in the atmosphere .1. Model development. *J. Geophys. Res.-Atmos.* **1997**, *102*, 3805–3818.
36. Lee, H. D.; Ray, K. K.; Tivanski, A. V. Solid, Semisolid, and Liquid Phase States of Individual Submicrometer Particles Directly Probed Using Atomic Force Microscopy. *Anal. Chem.* **2017**, *89*, 12720–12726.
37. Ovadnevaite, J.; Zuend, A.; Laaksonen, A.; Sanchez, K. J.; Roberts, G.; Ceburnis, D.; Decesari, S.; Rinaldi, M.; Hodas, N.; Facchini, M. C.; Seinfeld, J. H.; Dowd, C. O. Surface tension prevails over solute effect in organic-influenced cloud droplet activation. *Nature* **2017**, *546*, 637–641.
38. Koop, T.; Bookhold, J.; Shiraiwa, M.; Poschl, U. Glass transition and phase state of organic compounds: dependency on molecular properties and implications for secondary organic aerosols in the atmosphere. *Phys. Chem. Chem. Phys.* **2011**, *13*, 19238–55.
39. Power, R. M.; Simpson, S. H.; Reid, J. P.; Hudson, A. J. The transition from liquid to solid-like behaviour in ultrahigh viscosity aerosol particles. *Chem. Sci.* **2013**, *4*, 2597–2604.
40. Petters, M. D.; Kreidenweis, S. M. A single parameter representation of hygroscopic growth and cloud condensation nucleus activity. *Atmos. Chem. Phys.* **2007**, *7*, 1961–1971.
41. Ruehl, C. R.; Davies, J. F.; Wilson, K. R. An interfacial mechanism for cloud droplet formation on organic aerosols. *Science* **2016**, *351*, 1447–1450.
42. Ruehl, C. R.; Wilson, K. R. Surface Organic Mono layers Control the Hygroscopic Growth of Submicrometer Particles at High Relative Humidity. *J. Phys. Chem. A* **2014**, *118*, 3952–3966.
43. Lee, H. D.; Estillore, A. D.; Morris, H. S.; Ray, K. K.; Alejandro, A.; Grassian, V. H.; Tivanski, A. V. Direct Surface Tension Measurements of Individual Sub-Micrometer Particles Using Atomic Force Microscopy. *J. Phys. Chem. A* **2017**, *121*, 8296–8305.
44. Morris, H.; Grassian, V.; Tivanski, A. Humidity-dependent surface tension measurements of individual inorganic and organic submicrometre liquid particles. *Chem. Sci.* **2015**, *6*, 3242–3247.